HHS Public Access

Author manuscript

J Phys Chem B. Author manuscript; available in PMC 2020 June 20.

Published in final edited form as:

J Phys Chem B. 2019 June 20; 123(24): 5048–5058. doi:10.1021/acs.jpcb.9b02293.

Dynamic Nuclear Polarization Magic Angle Spinning NMR Combined with MD Simulations Permits Detection of Order and Disorder in Viral Assemblies

Rupal Gupta[1,3,#], **Huilan Zhang**[1,3], **Manman Lu**[1,3], **Guangjin Hou**[1,3], **Marc Caporini**[2,†], **Melanie Rosay**[2], **Werner Maas**[2], **Jochem Struppe**[2], **Jinwoo Ahn**[3,4], **In-Ja L. Byeon**[3,4], **Hartmut Oschkinat**[5], **Kristaps Jaudzems**[6], **Emeline Barbet-Massin**[6], **Lyndon Emsley**[7], **Guido Pintacuda**[6,*], **Anne Lesage**[6,*], **Angela M. Gronenborn**[3,4,*], **Tatyana Polenova**[1,3,*]

[1]Department of Chemistry and Biochemistry, University of Delaware, Newark, DE 19716, United States; [2]Bruker Biospin Corporation, 15 Fortune Drive, Billerica, MA 01821, United States; [3]Pittsburgh Center for HIV Protein Interactions, University of Pittsburgh School of Medicine, Pittsburgh, PA 15213, United States; [4]Department of Structural Biology, University of Pittsburgh School of Medicine, 3501 Fifth Ave., Pittsburgh, PA 15213, United States; [5]Leibniz-Institut für Molekulare Pharmakologie, Robert-Roessle-Str. 10, 13125 Berlin, Germany; [6]Centre de RMN à Très Hauts Champs, Institut des Sciences Analytiques, UMR 5280 CNRS / Ecole Normale Supérieure de Lyon, 5 rue de la Doua, 69100 Villeurbanne (Lyon), France; [7]Institut des Sciences et Ingénierie Chimques, Ecole Polytechnique Fédérale de Lausanne (EPFL), CH-1015 Lausanne, Switzerland;

Abstract

We report dynamic nuclear polarization (DNP) enhanced magic angle spinning (MAS) NMR spectroscopy in viral capsids from HIV-1 and bacteriophage AP205. Viruses regulate their lifecycles and infectivity through modulation of their structures and dynamics. While static structures of capsids from several viruses are now accessible with near-atomic level resolution, atomic-level understanding of functionally important motions in assembled capsids is lacking. We observed up to 64-fold signal enhancements by DNP, which permitted in-depth analysis of these assemblies. For the HIV-1 CA assemblies, remarkably high spectral resolution in the 3D and 2D

[*]**Corresponding authors:** Tatyana Polenova, Department of Chemistry and Biochemistry, University of Delaware, Newark, DE, USA, tpolenov@udel.edu; Angela M. Gronenborn, Department of Structural Biology, University of Pittsburgh School of Medicine, 3501 Fifth Ave., Pittsburgh, PA 15260, USA, amg100@pitt.edu; Anne Lesage, Centre de RMN à Très Hauts Champs, Institut des Sciences Analytiques, UMR 5280 CNRS / Ecole Normale Supérieure de Lyon, 5 rue de la Doua, 69100 Villeurbanne (Lyon), France, Anne.Lesage@ens-lyon.fr; Guido Pintacuda, Centre de RMN à Très Hauts Champs, Institut des Sciences Analytiques, UMR 5280 CNRS / Ecole Normale Supérieure de Lyon, 5 rue de la Doua, 69100 Villeurbanne (Lyon), France, guido.pintacuda@ens-lyon.fr.

[#]Present address: Department of Chemistry, College of Staten Island, Building 6S, Room 214, 2800 Victory Boulevard, Staten Island, NY 10314, United States;

[†]Present address: Amgen, Inc. 360 Binney St. Cambridge, MA 02142, United States

SUPPORTING INFORMATION INFORMATION

^{13}C and ^{15}N chemical shifts for resonances assigned with DNP-enhanced spectra, a plot showing differences in the chemical shifts for DNP and ambient temperature measurements and an overlay of simulated chemical shift distribution maps for all amino acid residues and the experimental DNP NCACX spectrum. This information can be found on the internet at http://pubs.acs.org.

COMPETING FINANCIAL INTERESTS

None of the authors have any competing financial interests.

heteronuclear datasets permitted the assignments of a significant fraction of backbone and side chain resonances. Using an integrated DNP MAS NMR and molecular dynamics simulations approach, the conformational space sampled by the assembled CA at cryogenic temperatures was mapped. Qualitatively, remarkable agreement was observed for the experimental $^{13}C/^{15}N$ chemical shift distributions and those calculated from substructures along the MD trajectory. Residues that are mobile at physiological temperatures are frozen out in multiple conformers at cryogenic conditions, resulting in broad experimental and calculated chemical shift distributions. Overall, our results suggest that DNP MAS NMR measurements in combination with MD simulations facilitate a thorough understanding of the dynamic signatures of viral capsids.

Graphical Abstract

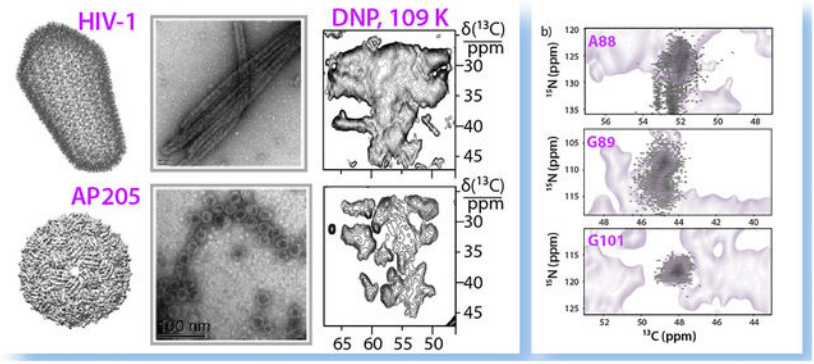

Keywords

magic angle spinning NMR; dynamic nuclear polarization; DNP; HIV-1 capsid; measles virus capsid; bacteriophage AP205 capsid; conformational dynamics

INTRODUCTION

Biological function is invariably connected to and depends on structure and dynamics of biological macromolecules and their complexes. Nuclear magnetic resonance (NMR) is one of the most powerful techniques to elucidate the intricate relationship between conformational flexibility and function, as, in contrast to X-ray diffraction and cryo-EM, it yields atomic-level information on both well-structured and dynamically disordered regions of individual biomolecules and assemblies. NMR experiments provide direct access to a number of site-specific experimental parameters (chemical shifts, residual anisotropic interactions, relaxation rates) that report directly on both structure and dynamics. These studies can be performed in solution on relatively small or flexible components, or on microcrystalline or sedimented assemblies under magic angle spinning (MAS) conditions.[1–13]

Typically, NMR experiments conducted at non-cryogenic temperatures provide dynamics information from averaged observables, reflecting the state of an ensemble of conformers, all of which contribute to the observable in a weighted manner. Solution NMR methods for studying dynamics are advanced, and ensemble analyses have been developed to describe

the conformational space and the timescale of the interconversions.[14–17] Extensive site-specific studies of dynamics in proteins and protein assemblies by solid-state NMR still remain relatively rare and challenging, often suffering from low sensitivity. The most commonly used approaches rely on the measurement of the various relaxation rates and their temperature dependencies,[18–20] relaxation dispersion curves,[21–22] dipolar and/or chemical shift anisotropy tensors,[2, 8, 13] and a combination of these methods.[23] These techniques yield information on motional rates and/or amplitudes and symmetries, over a broad range of timescales (see a recent review[24])

One example where motions are important in the regulation of biological function are virus capsids,[25] where dynamic regulation emerges as a key feature of assembly and disassembly, and of genome encapsidation. Local dynamics have been observed in large ordered assemblies and some viral capsids contain both ordered and disordered structural elements.[1326] Numerous recent solution NMR studies have described conformational disorder in viral proteins alone or in complex, such as paramyxoviral phosphoproteins, nucleoproteins, as well as HIV-1 Gag protein.[27–30] In a notable example, we probed dynamics of HIV-1 virus capsid assemblies and their interactions with the host factor Cyclophilin A (CypA)[13] by MAS NMR at temperatures close to physiological, where dynamically averaged experimental parameters were interpreted in light of those calculated from MD trajectories.[8, 13]

Here we explore an alternative approach based on dynamic nuclear polarization (DNP) enhanced MAS NMR spectroscopy at cryogenic temperatures and high magnetic fields to probe the conformational properties of large viral assemblies at atomic resolution and with high sensitivity. We examine two viral capsids: the human immunodeficiency 1 virus (HIV-1) capsid and the bacteriophage AP205 virus-like particles (VLPs). Viral capsids are unique compared to other classes of biomolecules, previously studied by DNP, such as amyloids or microcrystalline proteins studied by others previously,[31–32] because they are generally multicomponent assemblies that possess high curvature, often high symmetry and exhibit varying degrees of order and conformational flexibility.

In an earlier, pioneering study, Havlin and Tycko showed that ensembles of unfolded and partially-folded proteins could be trapped in glassy frozen solutions, and realized that 2D solid-state NMR lineshapes inform on the conformational distributions.[33] This approach suggested that MAS NMR spectra of frozen solutions might provide immediate access to the signatures of each individual conformer, and could be exploited in the context of dynamics studies to translate the dynamically averaged NMR parameters at room temperature into distributions of values.

Tycko's study was conducted at 9.4 T, a field where cross-peak lineshapes can be analyzed in terms of large conformational changes, as those induced by rapid chemical denaturation. However, conformational averaging in folded assemblies leads to subtler chemical shift distributions, which are masked by homogeneous broadening invariably accompanying MAS NMR spectra of biomolecules at cryogenic temperatures.[34] Here we show that this problem can be addressed by studying samples with DNP at high magnetic fields, leveraging a new generation of instruments operating at 14.1 T and above. On the one hand, DNP

drastically enhances the NMR signal, allowing the acquisition of 2D correlations in a matter of hours to days on few mgs of sample.[35–36] On the other hand, the combination of cryogenic temperatures and high magnetic fields yields 2D lineshapes that are dominated by inhomogeneous contributions.[37–40] facilitating their analysis in terms of rapid fluctuations within a conformational distribution using MD simulations.[41] This approach is well suited to probe the degree of dynamical disorder in these viral assemblies, and the associated motions can be quantified through an integrated DNP MAS NMR/MD simulations approach.

The level of detail elucidated in this study has been inaccessible even only a few years ago, and is now possible using high-field DNP and state-of-the-art MD simulations. We envision that the integrated approach described here will be particularly useful for characterizing minor species and mobile sites in viral assemblies as well as in other biological systems of comparable complexity.

MATERIALS AND METHODS

Sample Preparation.

Expression and purification of U-^{13}C, ^{15}N CA (HXB2 strain) was performed as reported previously.[9, 42] Tubular assemblies of CA were prepared from 32 mg/mL protein solutions in 25 mM phosphate buffer (pH 5.5) containing 2.4 M NaCl. The solutions were incubated at 37° C for 1 h and stored at 4° C for subsequent experiments. The samples for DNP enhanced measurements of CA tubular assemblies containing 8 mM AMUPol (15- {[(7-oxyl-3, 11-dioxa-7-azadispiro [5.1.5.3] hexadec- 15-yl) carbamoyl] [2-(2,5,8,11-tetraoxatridecan-13-ylamino)} - [3,11-dioxa-7-azadispiro [5.1.5.3] hexadec-7-yl]) oxidanyl)[43] were prepared as reported previously.[44] U-^{13}C, ^{15}N labeled MeV nucleocapsid was expressed and purified as reported elsewhere.[45–46] Samples for DNP-assisted measurements of MeV were prepared with 15 mM TOTAPOL ([1-(TEMPO-4-oxy)-3-(TEMPO-4-amino)propan-2-ol, where TEMPO = 2,2,6,6-tetramethylpiperidin-1-oxyl]).[47] To remove the C-terminal disordered tail and obtain cleaved MeV, intact MeV nucleocapsids were treated with trypsin (1 mg for 200 mg capsids, 45 min at room temperature)[48] and repurified by centrifugation through a 30% (v/v) glycerol cushion for 16 h at 77,000 g and 4 °C and subsequent dialysis against 50 mM potassium phosphate, 50 mM NaCl, pH 7.0. Samples for DNP-assisted measurements of cleaved MeV were prepared by suspending the pellet in 30 μl 15 mM TOTAPOL ([1-(TEMPO-4-oxy)-3-(TEMPO-4-amino)propan-2-ol, where TEMPO = 2,2,6,6-tetramethylpiperidin-1-oxyl]) dissolved in DNP juice (d_8-glycerol/D_2O/H_2O 60/30/10 v/v/v) and centrifuging into a 1.3 mm NMR rotor.[47] U-^{13}C, ^{15}N labeled microcrystalline AP205 nucleocapsid was prepared as described previously.[49] For DNP measurements, the crystals were soaked in 10 mM AMUPol solution in the crystallization mother liquor (0.1 M HEPES at pH 7.5, 0.1 M NaCl and 16% w/v deuterated PEG 4600) and then centrifuged into a 1.3 mm NMR rotor.

Transmission Electron Microscopy.

The sample morphologies were characterized by TEM analysis, performed in a Zeiss CEM 902 transmission electron microscope operating at 80 kV. Samples were stained with ammonium molybdate (5% w/v), deposited onto 400 mesh, formval/carbon-coated copper

grids, and dried for 40 min. Some of the assemblies were analyzed using a Zeiss Libra 120 transmission electron microscope operating at 120 kV. Samples were stained with uranyl acetate (5% w/v), deposited onto 400 mesh, formval/carbon-coated copper grids, and dried for 40 min in the air. The copper grids were pretreated with Pelco easiGlow Discharge Unit to deposit a charge, so that the assemblies were uniformly spread on the grid surface and adhered to it.

MAS NMR Spectroscopy.

19.96 T MAS NMR spectra of tubular assemblies of CA were acquired on a Bruker AVIII spectrometer equipped with a 3.2 mm E^{free} CPMAS HCN probe. The Larmor frequencies were 850.400 MHz (^{1}H) and 213.855 MHz (^{13}C). The spectra were collected at the MAS frequency of 14 kHz, and the temperature was maintained at 277 K. The typical pulse lengths were 2.9 μs for ^{1}H, 4.2 μs for ^{13}C. ^{1}H−^{13}C cross-polarization (CP) was performed with a linear amplitude ramp (80−100%); the CP contact time was 2 ms. The ^{13}C-^{13}C correlation spectrum was acquired using a COmbined $R2_n^v$– Driven (CORD)[50] experiment with a mixing time of 50 ms.

DNP-enhanced MAS NMR spectra of CA tubular assemblies were acquired in the Bruker Billerica laboratories on an Avance III SSNMR spectrometer equipped with a 3.2-mm triple-resonance low temperature MAS probe. At 14.1 T, the Larmor frequencies were 600.080 MHz (^{1}H), 150.905 MHz (^{13}C) and 60.813 MHz (^{15}N). The microwave (MW) frequency was 395.18 GHz and the MW irradiation generated by a second-harmonic gyrotron, which delivered 12 W of power at the sample. The measurements were performed at 109 K, and the sample temperature was calibrated using KBr.[51] The typical pulse lengths were 2.5 μs (^{1}H), 4 μs (^{13}C) and the ^{1}H-^{13}C contact time was 2 ms. All spectra were acquired at the MAS frequency of 12.5 kHz, controlled by a Bruker MAS controller. For 2D and 3D NCACX correlation experiments, band selective magnetization transfer from ^{15}N to ^{13}Cα was performed using a spectrally induced filtering in combination with cross polarization (SPECIFIC-CP)[52] contact time of 6.5 ms followed by a dipolar-assisted rotational resonance (DARR)[53–54] mixing time of 40 ms. For DNP-enhanced MAS NMR measurements at 18.8 T, the Larmor frequencies were 799.723 MHz (^{1}H) and 201.107 MHz (^{13}C), and the microwave frequency was 527 GHz. Data were recorded at a temperature of 110 K. The sample temperature was calibrated using KBr. The typical pulse lengths were 2.5 μs (^{1}H), 4.75 μs (^{13}C), and the ^{1}H-^{13}C CP contact time was 2 ms. The MAS frequency was 10 kHz, and the proton-driven spin diffusion (PDSD)[55] mixing time was 60 ms.

The DNP-assisted measurements on AP205 nucleocapsids were performed on a Bruker spectrometer equipped with a 1.3-mm triple resonance low temperature DNP probe at 18.8 T (Larmor frequencies: ^{13}C = 201.107 MHz, ^{1}H = 799.720 MHz). The CORD mixing time was 100 ms, the MAS frequency was 40 kHz and the temperature was 115 K.

Processing and Analysis of MAS NMR spectra.

The 2D NCACX and ^{13}C-^{13}C correlation spectra were processed in TopSpin using Gaussian and sine bell squared apodization applied to the direct and indirect dimension, respectively. The 3D NCACX spectrum was processed in NMRPipe[56] using 60° shifted sine bell

apodization, followed by a Lorentzian-to-Gaussian transformation in all dimensions. All data sets were analyzed in Sparky.[57]

Molecular Dynamics Simulations and Chemical Shift Predictions.

MD simulations for 100 ns were performed on CA monomer (HXB2 strain) as reported previously.[13] MD simulations of AP205 were performed on the dimeric subunit of the assembled capsid structure.[58] Bulk waters and sodium/chloride ions were added using VMD,[59] by setting the total concentration of NaCl to 0.15 M. The system was then equilibrated using ACEMD[60] for 2.1 ns at 300 K and the simulation was run for 100 ns. The chemical shifts for individual substructures of the trajectory were predicted using SHIFTX.[61]

RESULTS AND DISCUSSION

DNP MAS NMR Spectra of HIV-1 Capsids and AP205 VLPs: Disorder vs. Order

Mature HIV-1 capsids are cone-shape assemblies of ~1,500 copies of the 231-residue capsid (CA) protein (Fig. S1a, Supporting Information), a proteolytic cleavage product of Gag polyprotein. HIV-1 capsids hold the viral genome and the proteins necessary for viral replication.[62–63] The capsid cones are assembled from ~216 hexameric and 12 pentameric units of CA.[64–65] CA tubes, which have been studied extensively by cryo-EM[64–68] and MAS NMR spectroscopy,[3–4, 8–10, 13] capture the predominant symmetry element of the cones: a hexagonal lattice with six-fold symmetry, assembled from CA monomers (Fig. S1b, Supporting Information). In both conical and tubular assemblies, the N-terminal domains (NTDs) of CA (residues 1–149) form the outer surface of the tubular assemblies while the inner surface is lined by C-terminal domains (CTDs) (residues 150–231).

For HIV CA, it has been established by us and by others that conformational plasticity of CA, directly linked to its internal dynamics, is critical for capsid assembly,[8, 10,29,65,69–72] virus maturation,[9] and interactions with cellular host factors, such as CypA[13] and TRIM5α.[73] Atomic-level insights into the dynamics of the CA assemblies and its complexes with CypA and TRIM5α CC-SPRY domain were obtained by monitoring molecular motions on the nano- to millisecond timescales, using MAS NMR in combination with MD simulations.[8–9, 13, 73] These studies revealed that the functionally important CypA loop region is highly flexible.[8, 10, 13] These dynamics were found to be a determining factor in HIV-1's escape from CypA dependence. We also recently reported that broad signals from dynamically disordered regions of HIV-1 capsid protein assemblies,[44, 74] which are invisible at ambient temperatures, can be observed in frozen samples.[9, 13]

AP205 bacteriophages are small RNA viruses with an icosahedral capsid shell that is made up of 178 copies of the coat protein[49, 75] and a single copy of the maturation protein. In absence of the maturation protein, ninety dimers of the AP205 coat protein assemble into stable VLPs. Recently, a complete model of the AP205 VLP has been derived from a crystal structure of an unassembled coat protein dimer together with solid-state NMR and cryo-electron microscopy data (Fig 1e). This model revealed a circular permutation of the coat protein which allows both of its termini to be surface exposed in assembled VLPs tolerating

insertions at the N- or C- termini.[58] Despite the high level of characterization already available, the mechanism of assembly and genome encapsidation is not completely understood, and there is currently no information about the level of local dynamics that can be accommodated within icosahedral viral capsid assemblies. An atomic-level characterization of the structure and dynamics of viral particles is essential for understanding virus assembly, virus evolution, virus-host interactions and RNA genome recognition.

A comparison of ^{13}C-^{13}C correlation spectra of the two capsid assemblies acquired at ambient temperature (800 and 850 MHz) and under DNP conditions at 600 MHz (for HIV-1 CA) and 800 MHz (for AP205) field is shown in Fig. 1c,d and 1g,h. The ^{13}C resolution of the DNP-enhanced spectra acquired at around 109 K, while lower than that of the ambient temperature non-DNP data, is of the order of 1–1.8 ppm (as estimated from the resolved peaks in NCACX spectrum shown in Fig. 2b), which is considerably narrower than the DNP spectra of many proteins reported in the literature. Line broadening in DNP spectra can be caused by homogeneous and inhomogeneous contributions. The effects of homogeneous contributions to the line widths can be alleviated by increasing the strength of the static magnetic field, while the inhomogeneous contributions remain unaffected. As is evident in Fig. 1d and 1h, there are a number of resolved peaks corresponding to individual amino acids. Interestingly, the linewidths show variations from site to site. We hypothesized that the broader lines may be associated with the presence of motions and multiple conformers. We decided to explore this possibility further.

Heteronuclear DNP-Enhanced MAS NMR Spectra for HIV-1 CA Assemblies

The possible implications of dynamics observable in the DNP-enhanced MAS NMR spectra were first analyzed for HIV-1 CA assemblies. DNP-enhanced 2D MAS NMR spectra of tubular assemblies of HIV-1 CA and the Gag maturation intermediate containing CA and the 14-residue spacer peptide 1 (SP1), CA-SP1 were evaluated and 64 or 20-fold sensitivity enhancements at 109 K were obtained for CA and CA-SP1, respectively. This enabled time efficient acquisition of 2D homonuclear data sets and permitted detection of resonances for the flexible SP1 peptide region and determination of its secondary structure.[44] The resolution of these DNP-enhanced 2D homonuclear spectra was such that we could assign several sidechain and backbone resonances.[44] However, these data sets alone were insufficient for complete site-specific resonance assignments.

Therefore, 2D and 3D DNP-enhanced heteronuclear NCACX correlation spectra were recorded, which exhibit remarkably high resolution (Fig. 2). Furthermore, the acquisition time was only 0.6 and 17 hours for the 2D and 3D spectrum, respectively. Based on the 3D NCACX data set (Fig. 2a) and available chemical shifts from solution and MAS NMR studies,[4,76] backbone and the side chain resonances for 44 residues were obtained. The 2D NCACX spectrum of tubular CA assemblies and at 109 K (14.1 T) is displayed in Fig. 2b. Several well-resolved isolated resonances, particularly associated with the dynamic CypA-binding loop, were detected, similar to the 3D data set. In addition, resonances from several aromatic side chain atoms are seen in the spectra and were readily assigned. Resonances of

aromatic side chains generally exhibit low intensities in the ambient-temperature spectra, and their facile detection through DNP-based measurements is highly advantageous.

Spectral intensity is present for many amino acid residues of CA, as illustrated by the superposition of the NCACX spectra acquired under DNP and non-DNP conditions (Fig. 2c). Interestingly, resonances for several proline residues, which were not observed at ambient temperature, exhibited high intensities, and the chemical shifts indicate that both cis- and trans- conformers are present (Fig. S2, Supporting Information). The fact that we observed spectral intensity for most of the amino acids in both the NTD and CTD suggests that either the DNP biradical diffused into the tubes or that efficient spin diffusion from the exterior tube surface, lined by NTDs, to the interior lining of the tube, comprising CTDs, is present.

Overall, assignments were obtained for about 20 % of the total number of amino acids in the CA sequence (Fig. 2e). Residues with assigned resonances are highlighted on the structure of a single CA chain (Fig. 2f). Resonances for 10 residues in the CypA loop, which is located on the surface of the assemblies (Figure S1, Supporting Information) were assigned. The CypA loop residues are highly mobile at ambient temperatures, and we have characterized their dynamics extensively.[13] Therefore, the presence of the corresponding resonances in the DNP-enhanced spectra allows us to benchmark the approach for conformational space sampling using cryogenic temperature DNP data.

The temperature dependencies of the chemical shifts could be estimated from the DNP-enhanced spectra. Notably, chemical shift differences compared to ambient temperature spectra are observed (Fig. S3, Supporting Information), with larger than average differences (>1 ppm) occurring for resonances associated with mobile loops, compared to rigid regions. These large differences correlate with the reduced ^{1}H-^{15}N dipolar order parameters (Fig. S4–S5, Supporting Information), previously calculated on the basis of the MD trajectories.[13] Given that ^{1}H-^{15}N dipolar order parameters are sensitive to motions on the nano- to microsecond timescales, it appears that such motions can be indirectly inferred by examining the chemical shift differences at cryogenic conditions. This possibility is further explored below.

Residue-specific Conformational Space Mapping by Combining DNP MAS NMR and MD Simulations

The possibility of exploiting spectral broadening introduced by conformational heterogeneity in DNP-enhanced spectra as a possible probe of dynamics was first explored for CA assemblies. The resolution of the DNP MAS NMR spectra of CA tubular assemblies is relatively high, compared to DNP spectra for the majority of other biological systems to date.[44] Nevertheless, as mentioned previously, with typical carbon-13 peak widths of 1.0 ppm up to 1.8 ppm, resolution is still considerably lower than in the ambient-temperature spectra.[13, 44] Two factors have been shown previously to contribute to signal broadening and attenuation of intensities in DNP-enhanced measurements: conformational heterogeneity[34, 41, 77–78] and paramagnetic relaxation enhancements (PREs) due to the presence of biradical.[39, 41, 79] The latter has been observed at ambient temperature for solvent exposed regions of K^{+} channel integrated into membranes.[41] In our current study on

tubular CA assemblies, relatively small increases in line widths were detected in ^{13}C-^{13}C homonuclear experiments at ambient temperatures,[44] therefore, although the DNP spectra are recorded at a different temperature, PREs are not expected to be a significant source of signal broadening in the current DNP studies.

Conformational heterogeneity is characterized by the presence of distinct conformers that are in dynamic exchange at ambient temperatures but are individually observable at cryogenic temperatures due to reduced molecular motions. As a result, line broadening in DNP-assisted spectra is expected to be residue-specific and difficult to predict without prior knowledge of the implicated motions. In general, the set of conformers that can contribute to each observable signal depends on multiple factors, such as the conformational space sampled by the individual residues, the interaction of side chains with solvent molecules in the frozen matrix, and the individual rates of the associated exchange/motional processes. Solvent molecules in the frozen, glassy state will interact with amino acid side chains differently than in ambient temperature solution. In a typical DNP experiment, the sample is slowly frozen to the desired cryogenic temperature with cooling rates as low as 1°/min[34] or as high as 10°/s.[77] An earlier study by Tycko and coworkers reported that while these slow freezing conditions trap equilibrium conformations, if a system is frozen quickly (e.g., freeze-quenching by spraying a solution of a protein under investigation into cold isopenthane) non-equilibrium states are additionally trapped, and mixtures of unfolded and fully folded molecules were found to be present.[80] Therefore, the subset of conformers present in the DNP NMR experiments here is anticipated to reflect equilibrium distribution of conformers.

MD simulations could potentially provide valuable information about the accessible conformational space and, within the practically reachable simulation timescales, should inform on the equilibrium conformations trapped under the slow-freezing conditions employed in this work. Indeed, the chemical shift distributions derived on the basis of the MD trajectory show good agreement with experimental DNP MAS NMR results. The Baldus group has previously used MD trajectories to estimate 1D ^{13}C lineshapes from DNP-based experiments.[41] Here, we calculated chemical shifts from individual frames of the MD trajectories to obtain the distribution of conformers compatible with the observed shifts in 2D DNP MAS NMR experiments. To this end, 5000 frames were extracted from a 100 ns MD trajectory for CA tubular assemblies.

The effect of conformational heterogeneity in 2D heteronuclear DNP spectra of CA tubular assemblies is examined in Fig. 3a, which depicts $^{13}C^{\alpha}$ and $^{15}N^{H}$ chemical shift distributions for the sets of conformers observed for eight representative residues whose cross peaks are sufficiently resolved for the analysis, extracted from the MD conformer ensemble. The distribution of chemical shift values over the course of the MD trajectory is displayed in Fig. 3a. Not surprisingly, residues that reside in the flexible CypA loop (e.g., A88 and G89) exhibit broader chemical shift distributions than those in more rigid regions, such as G116. This is qualitatively borne out by our data: the degree of molecular motion (as determined by the extent of the attenuation of dipolar order parameters with respect to the rigid limit values) correlates with the chemical shift distribution width, see Fig. S4 of the Supporting

Information. Dynamic residues, such as A88 and G89, exhibit broader chemical shift distributions compared to rigid residues, such as A105, S109 and G116.

Furthermore, the variability in $^{15}N^{H}$ chemical shifts is larger than in $^{13}C^{\alpha}$ shifts, both based on the MD simulations (Fig. 3a), as well as experimentally (Fig. 2d), suggesting that conformational heterogeneity will result in more extensive broadening in the ^{15}N dimension than in the ^{13}C dimension. In contrast, the line widths (in ppm) in the non-DNP spectra acquired at ambient conditions are very similar in the ^{15}N and ^{13}C dimensions. Therefore, the overall non-uniform increase in signal widths under DNP conditions is a strong indication that the predominant underlying cause for broadening is conformational heterogeneity, directly related to the relative flexibility of individual residues. Consequently, without the knowledge of the conformational space that is sampled by an individual residue, the extent of spectral broadening is difficult to predict. However, it becomes accessible through MD simulations.

To test the above assertion further, experimental 2D DNP lineshapes were compared with those simulated on the basis of the individual conformers in the MD trajectory for several representative residues. The simulated chemical shift distributions for every pair of $^{13}C^{\alpha}$ and $^{15}N^{H}$ chemical shifts based on 5000 snapshots of a 100 ns MD trajectory are weighted with respect to abundance: the higher the frequency of a particular chemical shift pair, the brighter the spot (Fig. 3b). The agreement between the simulated and the experimental contour maps is generally very good and is applicable to both rigid residues (G101, I104, A105, G106, S109, and G116) and dynamic residue, G89. A superposition of the chemical shift distribution map generated for all amino acids and the experimental DNP-enhanced NCACX spectrum is provided in Fig. S6, Supporting Information. The agreement of the experimental shifts with the MD-derived chemical shift maps suggests that the conformers captured by MD are representative of the accessible conformational space, despite the fact that the sample freezing rates were slow in the current study. Indirectly, this assertion is supported by the fact that the use of shorter MD trajectories (up to 10 ns) does not reproduce the breadth of the observed chemical shift distributions for dynamic residues, as illustrated in Fig. S7, Supporting Information.

Not for all residues is a quantitative agreement observed. For example, for the dynamic A88 residue the experimental and calculated shifts are different. This discrepancy cannot be explained by a PRE effect, since no line broadening is observed, and the experimental peaks are narrower than the calculated distributions. One possibility may be that not all conformers can be frozen out during the slow cooling, although this hypothesis remains to be tested. Interestingly, the experimental ^{1}H-^{15}N dipolar order parameters for A88 at 4°C also indicated that this residue is less dynamic than predicted by MD simulations ($S^{exp} = 0.39$ vs $S^{MD} = 0.11$ for the ^{1}H-^{15}N bond).[13] Furthermore, PRE-induced spectral broadening is expected to be relatively homogeneous, which is not borne out in the comparison of the simulated and experimental lineshapes (Fig. 3), and the presence or absence of the PRE effect may depend on the morphology of the sample, the nature and the concentration of the biradical.[41,79,81]

The different extents to which $^{13}C^{\alpha}$and$^{15}N^{H}$ chemical shifts are affected by dynamics, as observed experimentally and through MD simulations, demonstrates that both of these nuclei should be taken into consideration when analyzing the conformational space from experiments conducted at cryogenic temperatures, where molecular motions are restricted. Such an analysis will potentially allow for estimating the entire conformational space and dynamics in HIV-1 protein and other viral assemblies and will be pursed in conjunction with detailed studies aimed at estimating the relative contributions of PRE-induced or conformational heterogeneity-associated spectral broadening in the future.

Intact Viral Assemblies: Bacteriophage AP205

Intrigued by the findings on the HIV-1 CA assemblies, we examined the ^{13}C chemical shift distributions in the VLPs of the bacteriophage AP205 coat protein, on the basis of 1000 frames extracted from a 100 ns MD trajectory. Resonance assignments derived from the 2D DNP-enhanced spectra were validated by the comparison with the assignments reported by us previously on the basis of the 2D and 3D spectra acquired at 275 K,[58] with minor temperature-induced chemical shift changes. A superposition of the experimental 2D ^{13}C-^{13}C correlation spectra with the simulated chemical shift distribution maps is provided in Fig. 4. Qualitatively, the simulated chemical shift distributions for AP205 exhibit reasonable agreement with the experimental spectra, suggesting that conformers in the MD trajectories, which would be averaged at ambient temperatures, are trapped and become detectable at cryogenic temperatures in the DNP experiments. It is worth noting that for AP205 the analysis was performed for C^{α}-C^{β} correlations, while for the HIV-1 CA – for the N^{H}-C^{α} correlations between the backbone atoms. This may explain why the agreement is slightly less convincing than for the lineshapes presented in Fig. 3

The approach presented here is in its early stages of development and has inherent limitations, such as i) the lack of clear procedure, at the current time, to assure that the states trapped at cryogenic temperatures represent all of the equilibrium conformers; and ii) MD simulations sample the entire equilibrium conformational space. To gain systematic understanding into these issues and to overcome these, further investigations are needed spanning multiple systems and multiple conditions.

CONCLUSIONS

We applied an integrated DNP MAS NMR/MD approach for analyzing structure and dynamics in HIV-1 capsid assemblies and bacteriophage AP205 VLPs. The study was enabled by DNP-enhanced MAS NMR spectroscopy that yielded considerable sensitivity gains. It was then possible to record 2D and 3D heteronuclear correlation spectra in a fraction of time, compared to the acquisition of conventional data sets. We show that at low temperatures individual conformers, which are in dynamic exchange at ambient temperatures, are frozen out such that they exhibit separate lines in ^{13}C and ^{15}N NMR spectra. The detected, distinct $^{13}C/^{15}N$ chemical shift distributions are in accord with the extent of dynamics and the accessible conformational space in HIV-1 CA and AP205 assemblies displayed by the chemical shift distributions, calculated from MD trajectories. Remarkable qualitative agreement between the ^{15}N and ^{13}C 2D lineshapes and calculated

chemical shift distributions is observed. Our results suggest that DNP-based experiments combined with MD simulations can be used to probe both structure and conformational dynamics. Furthermore, the integrated methodology described here is a powerful means to study functionally relevant dynamics in complex biological systems, including but not limited to viruses.

Supplementary Material

Refer to Web version on PubMed Central for supplementary material.

ACKNOWLEDGMENTS

This work was supported by the National Institutes of Health (NIH Grant-P50GM082251 to AMG and TP) and is a contribution from the Pittsburgh Center for HIV Protein Interactions, and by GRAL (ANR-10-LABX-49–01) and Finovi (Fondation innovations en infectiologie). We acknowledge the support of the NSF CHE0959496 grant for acquisition of the 850 MHz NMR spectrometer and of the NIGMS P30 GM110758–01 grant for the support of core instrumentation infrastructure at the University of Delaware. We thank Professor Christopher J. Langmead at the Carnegie Mellon University for providing MD trajectories of CA monomer. The work used the platforms of the Grenoble Instruct-ERIC centre (ISBG; UMS 3518 CNRS-CEA-UJA-EMBL) with support from FRISBI (ANR-10-INSB-05–02) and GRAL (ANR-10-LABX-49–01) within the Grenoble Partnership for Structural Biology (PSB). The electron microscope facility is supported by the Rhône-Alpes Region, the Fondation Recherche Medicale (FRM), the fonds FEDER, the Centre National de la Recherche Scientifique (CNRS), the CEA, the University of Grenoble, EMBL, and the GIS-Infrastructures en Biologie Sante et Agronomie (IBISA). We thank Fenel Daphna, Drs. Christine Moriscot and Guy Schoehn, from the Electron Microscopy platform of the Integrated Structural Biology of Grenoble (ISBG, UMS 3518). We thank the European Synchrotron Radiation Facility (ESRF).

REFERENCES

1. Goldbourt A; Gross BJ; Day LA; McDermott AE, Filamentous Phage Studied by Magic-Angle Spinning NMR: Resonance Assignment and Secondary Structure of the Coat Protein in Pf1. J. Am. Chem. Soc 2007, 129, 2338–2344. [PubMed: 17279748]
2. Lorieau JL; Day LA; McDermott AE, Conformational Dynamics of an Intact Virus: Order Parameters for the Coat Protein of Pf1 Bacteriophage. Proc. Natl. Acad. Sci. USA 2008, 105, 10366–10371. [PubMed: 18653759]
3. Chen B; Tycko R, Structural and Dynamical Characterization of Tubular HIV-1 Capsid Protein Assemblies by Solid State Nuclear Magnetic Resonance and Electron Microscopy. Protein Sci 2010, 19, 716–730. [PubMed: 20095046]
4. Han Y; Ahn J; Concel J; Byeon IJL; Gronenborn AM; Yang J; Polenova T, Solid-State NMR Studies of HIV-1 Capsid Protein Assemblies. J. Am. Chem. Soc 2010, 132, 1976–1987. [PubMed: 20092249]
5. Morag O; Abramov G; Goldbourt A, Similarities and Differences within Members of the Ff Family of Filamentous Bacteriophage Viruses. J. Phys. Chem. B 2011, 115, 15370–15379. [PubMed: 22085310]
6. Abramov G; Morag O; Goldbourt A, Magic-Angle Spinning NMR of a Class I Filamentous Bacteriophage Virus. J. Phys. Chem. B 2011, 115, 9671–9680. [PubMed: 21702439]
7. Sergeyev IV; Day LA; Goldbourt A; McDermott AE, Chemical Shifts for the Unusual DNA Structure in Pf1 Bacteriophage from Dynamic-Nuclear-Polarization-Enhanced Solid-State NMR Spectroscopy. J. Am. Chem. Soc 2011, 133, 20208–20217. [PubMed: 21854063]
8. Byeon IJL; Hou G; Han Y; Suiter CL; Ahn J; Jung J; Byeon CH; Gronenborn AM; Polenova T, Motions on the Millisecond Time Scale and Multiple Conformations of HIV-1 Capsid Protein: Implications for Structural Polymorphism of CA Assemblies. J. Am. Chem. Soc 2012, 134, 6455–6466. [PubMed: 22428579]
9. Han Y; Hou G; Suiter CL; Ahn J; Byeon IJL; Lipton AS; Burton S; Hung I; Gor'kov PL; Gan ZH, et al., Magic Angle Spinning NMR Reveals Sequence-Dependent Structural Plasticity, Dynamics, and

the Spacer Peptide 1 Conformation in HIV-1 Capsid Protein Assemblies. J. Am. Chem. Soc 2013, 135, 17793–17803. [PubMed: 24164646]

10. Bayro MJ; Chen B; Yau WM; Tycko R, Site-Specific Structural Variations Accompanying Tubular Assembly of the HIV-1 Capsid Protein. J. Mol. Biol 2014, 426, 1109–1127. [PubMed: 24370930]
11. Morag O; Abramov G; Goldbourt A, Complete Chemical Shift Assignment of the ssDNA in the Filamentous Bacteriophage fd Reports on Its Conformation and on Its Interface with the Capsid Shell. J. Am. Chem. Soc 2014, 136, 2292–2301. [PubMed: 24447194]
12. Barbet-Massin E; Felletti M; Schneider R; Jehle S; Communie G; Martinez N; Jensen MR; Ruigrok RWH; Emsley L; Lesage A, et al., Insights into the Structure and Dynamics of Measles Virus Nucleocapsids by H-1-detected Solid-state NMR. Biophys. J 2014, 107, 941–946. [PubMed: 25140429]
13. Lu M; Hou G; Zhang HL; Suiter CL; Ahn J; Byeon IJL; Perilla JR; Langmead CJ; Hung I; Gor'kov PL, et al., Dynamic Allostery Governs Cyclophilin A-HIV Capsid Interplay. Proc. Natl. Acad. Sci. USA 2015, 112, 14617–14622. [PubMed: 26553990]
14. Palmer AG 3rd, NMR Probes of Molecular Dynamics: Overview and Comparison with Other Techniques. Annu. Rev. Biophys. Biomol. Struct 2001, 30, 129–55. [PubMed: 11340055]
15. Palmer AG 3rd, Enzyme Dynamics from NMR Spectroscopy. Acc. Chem. Res 2015, 48, 457–65. [PubMed: 25574774]
16. Salmon L; Blackledge M, Investigating Protein Conformational Energy Landscapes and Atomic Resolution Dynamics from NMR Dipolar Couplings: a Review. Rep. Prog. Phys 2015, 78, 126601. [PubMed: 26517337]
17. Lisi GP; Loria JP, Using NMR Spectroscopy to Elucidate the Role of Molecular Motions in Enzyme Function. Prog. Nucl. Magn. Reson. Spectrosc 2016, 92–93, 1–17.
18. Williams JC; McDermott AE, Dynamics of the Flexible Loop of Triosephosphate Isomerase: the Loop Motion is Not Ligand Gated. Biochemistry 1995, 34, 8309–19. [PubMed: 7599123]
19. Quinn CM; McDermott AE, Quantifying Conformational Dynamics Using Solid-State $R_{1\rho}$ Experiments. J. Magn. Reson 2012, 222, 1–7. [PubMed: 22820004]
20. Lewandowski JR; Halse ME; Blackledge M; Emsley L, Direct Observation of Hierarchical Protein Dynamics. Science 2015, 348, 578–81. [PubMed: 25931561]
21. Tollinger M; Sivertsen AC; Meier BH; Ernst M; Schanda P, Site-Resolved Measurement of Microsecond-to-Millisecond Conformational-Exchange Processes in Proteins by Solid-State NMR Spectroscopy. J. Am. Chem. Soc 2012, 134, 14800–7. [PubMed: 22908968]
22. Krushelnitsky A; Gauto D; Rodriguez Camargo DC; Schanda P; Saalwachter K, Microsecond Motions Probed by Near-Rotary-Resonance $R_{1\rho}$ ^{15}N MAS NMR Experiments: The Model Case of Protein Overall-Rocking in Crystals. J. Biomol. NMR 2018, 71, 53–67. [PubMed: 29845494]
23. Zinkevich T; Chevelkov V; Reif B; Saalwachter K; Krushelnitsky A, Internal Protein Dynamics on ps to μs Timescales as Studied by Multi-frequency ^{15}N Solid-State NMR Relaxation. J. Biomol. NMR 2013, 57, 219–35. [PubMed: 24048638]
24. Quinn CM; Polenova T, Structural Biology of Supramolecular Assemblies by Magic-Angle Spinning NMR Spectroscopy. Q. Rev. Biophys 2017, 50, 1–44.
25. Mateu MG, Assembly, Stability and Dynamics of Virus Capsids. Arch. Biochem. Biophys 2013, 531, 65–79. [PubMed: 23142681]
26. Milles S; Jensen MR; Lazert C; Guseva S; Ivashchenko S; Communie G; Maurin D; Gerlier D; Ruigrok RWH; Blackledge M, An ultraweak interaction in the intrinsically disordered replication machinery is essential for measles virus function. Science Advances 2018, 4, eaat7778. [PubMed: 30140745]
27. Jensen MR; Bernado P; Houben K; Blanchard L; Marion D; Ruigrok RW; Blackledge M, Structural Disorder within Sendai Virus Nucleoprotein and Phosphoprotein: Insight into the Structural Basis of Molecular Recognition. Protein Pept. Lett 2010, 17, 952–60. [PubMed: 20450486]
28. Labaronne A; Milles S; Donchet A; Jensen MR; Blackledge M; Bourhis JM; Ruigrok RWH; Crepin T, Structural Analysis of the Complex between Influenza B Nucleoprotein and Human Importin-Alpha. Sci. Rep 2017, 7, 17164. [PubMed: 29215074]

29. Deshmukh L; Ghirlando R; Clore GM, Conformation and Dynamics of the Gag Polyprotein of the Human Immunodeficiency Virus 1 Studied by NMR Spectroscopy. Proc. Natl. Acad. Sci. USA 2015, 112, 3374–9. [PubMed: 25713345]
30. Baronti L; Erales J; Habchi J; Felli IC; Pierattelli R; Longhi S, Dynamics of the Intrinsically Disordered C-Terminal Domain of the Nipah Virus Nucleoprotein and Interaction with the X Domain of the Phosphoprotein as Unveiled by NMR Spectroscopy. ChemBioChem 2015, 16, 268–76. [PubMed: 25492314]
31. Debelouchina GT; Bayro MJ; Fitzpatrick AW; Ladizhansky V; Colvin MT; Caporini MA; Jaroniec CP; Bajaj VS; Rosay M; Macphee CE, et al., Hgher Order Amyloid Fibril Structure by MAS NMR and DNP Spectroscopy. J. Am. Chem. Soc 2013, 135, 19237–19247. [PubMed: 24304221]
32. Geiger M-A; Orwick-Rydmark M; Märker K; Franks WT; Akhmetzyanov D; Stöppler D; Zinke M; Specker E; Nazaré M; Diehl A, et al., Temperature Dependence of Cross-Effect Dynamic Nuclear Polarization in Rotating Solids: Advantages of Elevated Temperatures. PCCP 2016, 18, 30696–30704. [PubMed: 27791210]
33. Havlin RH; Tycko R, Probing Site-Specific Conformational Sistributions in Protein Folding with Solid-State NMR. Proc. Natl. Acad. Sci. USA 2005, 102, 3284–9. [PubMed: 15718283]
34. Linden AH; Franks WT; Akbey U; Lange S; van Rossum BJ; Oschkinat H, Cryogenic Temperature Effects and Resolution Upon Slow Cooling of Protein Preparations in Solid State NMR. J. Biomol. NMR 2011, 51, 283–92. [PubMed: 21826519]
35. Ni QZ; Daviso E; Can TV; Markhasin E; Jawla SK; Swager TM; Temkin RJ; Herzfeld J; Griffin RG, High Frequency Dynamic Nuclear Polarization. Acc. Chem. Res 2013, 46, 1933–1941. [PubMed: 23597038]
36. Akbey Ü; Oschkinat H, Structural Biology Applications of Solid-State MAS DNP NMR. Perspect. Magn. Reson 2016, 269, 213–224.
37. Sergeyev IV; Itin B; Rogawski R; Day LA; McDermott AE, Efficient Assignment and NMR Analysis of an Intact Virus Using Sequential Side-Chain Correlations and DNP Sensitization. Proc. Natl. Acad. Sci. USA 2017, 114, 5171–5176. [PubMed: 28461483]
38. Fricke P; Mance D; Chevelkov V; Giller K; Becker S; Baldus M; Lange A, High Resolution Observed in 800 MHz DNP Spectra of Extremely Rigid Type III Secretion Needles. J. Biomol. NMR 2016, 65, 121–6. [PubMed: 27351550]
39. Jaudzems K; Bertarello A; Chaudhari SR; Pica A; Cala-De Paepe D; Barbet-Massin E; Pell AJ; Akopjana I; Kotelovica S; Gajan D, et al., Dynamic Nuclear Polarization-Enhanced Biomolecular NMR Spectroscopy at High Magnetic Field with Fast Magic-Angle Spinning. Angew. Chem. Int. Ed. Engl 2018, 57, 7458–7462. [PubMed: 29566299]
40. Uluca B; Viennet T; Petrovic D; Shaykhalishahi H; Weirich F; Gonulalan A; Strodel B; Etzkorn M; Hoyer W; Heise H, DNP-Enhanced MAS NMR: A Tool to Snapshot Conformational Ensembles of alpha-Synuclein in Different States. Biophys. J 2018, 114, 1614–1623. [PubMed: 29642031]
41. Koers EJ; van der Cruijsen EA; Rosay M; Weingarth M; Prokofyev A; Sauvee C; Ouari O; van der Zwan J; Pongs O; Tordo P, et al., NMR-Based Structural Biology Enhanced by Dynamic Nuclear Polarization at High Magnetic Field. J. Biomol. NMR 2014, 60, 157–68. [PubMed: 25284462]
42. Sun SJ; Han Y; Paramasivam S; Yan S; Siglin AE; Williams JC; Byeon IJL; Ahn J; Gronenborn AM; Polenova T, Solid-State NMR Spectroscopy of Protein Complexes. Methods Mol. Biol 2012, 831, 303–331. [PubMed: 22167681]
43. Sauvée C; Rosay M; Casano G; Aussenac F; Weber RT; Ouari O; Tordo P, Highly Efficient, Water-Soluble Polarizing Agents for Dynamic Nuclear Polarization at High Frequency. Angew. Chem. Int. Ed 2013, 52, 10858–10861.
44. Gupta R; Lu M; Hou G; Caporini MA; Rosay M; Maas W; Struppe J; Suiter C; Ahn J; Byeon IJ, et al., Dynamic Nuclear Polarization Enhanced MAS NMR Spectroscopy for Structural Analysis of HIV-1 Protein Assemblies. J. Phys. Chem. B 2016, 120, 329–39. [PubMed: 26709853]
45. Desfosses A; Goret G; Estrozi LF; Ruigrok RWH; Gutsche I, Nucleoprotein-RNA Orientation in the Measles Virus Nucleocapsid by Three-Dimensional Electron Microscopy. J. Virol 2011, 85, 1391–1395. [PubMed: 21106738]

46. Jensen MR; Communie G; Ribeiro EA; Martinez N; Desfosses A; Salmon L; Mollica L; Gabel F; Jamin M; Longhi S, et al., Intrinsic Disorder in Measles Virus Nucleocapsids. Proc. Natl. Acad. Sci. USA 2011, 108, 9839–9844. [PubMed: 21613569]
47. Song CS; Hu KN; Joo CG; Swager TM; Griffin RG, TOTAPOL: A Biradical Polarizing Agent for Dynamic Nuclear Polarization Experiments in Aqueous Media. J. Am. Chem. Soc 2006, 128, 11385–11390. [PubMed: 16939261]
48. Schoehn G; Mavrakis M; Albertini A; Wade R; Hoenger A; Ruigrok RWH, The 12 Å Structure of Trypsin-treated Measles Virus N–RNA. J. Mol. Biol 2004, 339, 301–312. [PubMed: 15136034]
49. Andreas LB; Jaudzems K; Stanek J; Lalli D; Bertarello A; Le Marchand T; Cala-De Paepe D; Kotelovica S; Akopjana I; Knott B, et al., Structure of Fully Protonated Proteins by Proton-Detected Magic-Angle Spinning NMR. Proc. Natl. Acad. Sci. USA 2016, 113, 9187–9192. [PubMed: 27489348]
50. Hou G; Yan S; Trébosc J; Amoureux JP; Polenova T, Broadband Homonuclear Correlation Spectroscopy Driven by Combined R2nv Sequences under Fast Magic Angle Spinning for NMR Structural Analysis of Organic and Biological Solids. J. Magn. Reson 2013, 232, 18–30. [PubMed: 23685715]
51. Thurber KR; Tycko R, Measurement of Sample Temperatures under Magic-Angle Spinning from the Chemical Shift and Spin-Lattice Relaxation Rate of ^{79}Br in KBr Powder. J. Magn. Reson 2009, 196, 84–87. [PubMed: 18930418]
52. Baldus M; Petkova AT; Herzfeld J; Griffin RG, Cross Polarization in the Tilted Frame: Assignment and Spectral Simplification in Heteronuclear Spin Systems. Mol. Phys 1998, 95, 1197–1207.
53. Takegoshi K; Nakamura S; Terao T, ^{13}C-^{1}H Dipolar-Assisted Rotational Resonance in Magic-Angle Spinning NMR. Chem. Phys. Lett 2001, 344, 631–637.
54. Takegoshi K; Nakamura S; Terao T, ^{13}C-^{1}H Dipolar-Driven ^{13}C-^{13}C Recoupling Without ^{13}C RF Irradiation in Nuclear Magnetic Resonance of Rotating Solids. J. Chem. Phys 2003, 118, 2325–2341.
55. Bloembergen N, On the Interaction of Nuclear Spins in a Crystalline Lattice. Physica 1949, 15, 386–426.
56. Delaglio F; Grzesiek S; Vuister GW; Zhu G; Pfeifer J; Bax A, NMRPipe - a Multidimensional Spectral Processing System Based on Unix Pipes. J. Biomol. NMR 1995, 6, 277–293. [PubMed: 8520220]
57. Goddard TD; Kneller DG SPARKY, version 3.114; University of California, San Francisco, 2008.
58. Shishovs M; Rumnieks J; Diebolder C; Jaudzems K; Andreas LB; Stanek J; Kazaks A; Kotelovica S; Akopjana I; Pintacuda G, et al., Structure of AP205 Coat Protein Reveals Circular Permutation in ssRNA Bacteriophages. J. Mol. Biol 2016, 428, 4267–4279. [PubMed: 27591890]
59. Humphrey W; Dalke A; Schulten K, VMD: Visual Molecular Dynamics. J. Mol. Graphics 1996, 14, 33–8, 27–8.
60. Harvey MJ; Giupponi G; Fabritiis GD, ACEMD: Accelerating Biomolecular Dynamics in the Microsecond Time Scale. J. Chem. Theor. Comput 2009, 5, 1632–1639.
61. Neal S; Nip AM; Zhang HY; Wishart DS, Rapid and Accurate Calculation of Protein ^{1}H, ^{13}C and ^{15}N chemical shifts. J. Biomol. NMR 2003, 26, 215–240. [PubMed: 12766419]
62. Engelman A; Cherepanov P, The Structural Biology of HIV-1: Mechanistic and Therapeutic Insights. Nat. Rev. Microbiol 2012, 10, 279–90. [PubMed: 22421880]
63. Freed EO, HIV-1 Assembly, Release and Maturation. Nat. Rev. Microbiol 2015, 13, 484–96. [PubMed: 26119571]
64. Ganser-Pornillos BK; Cheng A; Yeager M, Structure of Full-Length HIV-1CA: A Model for the Mature Capsid Lattice. Cell 2007, 131, 70–79. [PubMed: 17923088]
65. Zhao GP; Perilla JR; Yufenyuy EL; Meng X; Chen B; Ning JY; Ahn J; Gronenborn AM; Schulten K; Aiken C, et al., Mature HIV-1 Capsid Structure by Cryo-Electron Microscopy and All-Atom Molecular Dynamics. Nature 2013, 497, 643–646. [PubMed: 23719463]
66. Ganser BK; Li S; Klishko VY; Finch JT; Sundquist WI, Assembly and Analysis of Conical Models for the HIV-1 Core. Science 1999, 283, 80–3. [PubMed: 9872746]
67. Li S; Hill CP; Sundquist WI; Finch JT, Image Reconstructions of Helical Assemblies of the HIV-1 CA Protein. Nature 2000, 407, 409–13. [PubMed: 11014200]

68. Byeon IJL; Meng X; Jung JW; Zhao GP; Yang RF; Ahn JW; Shi J; Concel J; Aiken C; Zhang PJ, et al., Structural Convergence between Cryo-EM and NMR Reveals Intersubunit Interactions Critical for HIV-1 Capsid Function. Cell 2009, 139, 780–790. [PubMed: 19914170]
69. Chen B; Tycko R, Simulated Self-Assembly of the HIV-1 Capsid: Protein Shape and Native Contacts Are Sufficient for Two-Dimensional Lattice Formation. Biophys. J 2011, 100, 3035–3044. [PubMed: 21689538]
70. Deshmukh L; Schwieters CD; Grishaev A; Ghirlando R; Baber JL; Clore GM, Structure and Dynamics of Full-Length HIV-1 Capsid Protein in Solution. J. Am. Chem. Soc 2013, 135, 16133–47. [PubMed: 24066695]
71. Müller B; Krijnse-Locker J, Imaging of HIV Assembly and Release. Methods Mol. Biol 2014, 1087, 167–184. [PubMed: 24158822]
72. Gres AT; Kirby KA; KewalRamani VN; Tanner JJ; Pornillos O; Sarafianos SG, X-ray Crystal Structures of Native HIV-1 Capsid Protein Reveal Conformational Variability. Science 2015, 349, 99–103. [PubMed: 26044298]
73. Quinn CM; Wang M; Fritz MP; Runge B; Ahn J; Xu C; Perilla JR; Gronenborn AM; Polenova T, Dynamic Regulation of HIV-1 Capsid Interaction with the Restriction Factor TRIM5α Identified by Magic Angle Spinning NMR and MD Simulations. Proc. Natl. Acad. Sci. USA 2018, ePub ahead of print.
74. Wang M; Quinn CM; Perilla JR; Zhang H; Shirra R Jr.; Hou G; Byeon IJ; Suiter CL; Ablan S; Urano E, et al., Quenching Protein Dynamics Interferes with HIV Capsid Maturation. Nat. Commun 2017, 8, 1779. [PubMed: 29176596]
75. Koning RI; Gomez-Blanco J; Akopjana I; Vargas J; Kazaks A; Tars K; Carazo JM; Koster AJ, Asymmetric cryo-EM reconstruction of phage MS2 reveals genome structure in situ. Nature Communications 2016, 7, 12524.
76. Jung J; Byeon IJ; Ahn J; Concel J; Gronenborn AM, ^{1}H, ^{15}N and ^{13}C Assignments of the Dimeric C-Terminal Domain of HIV-1 Capsid Protein. Biomol. NMR Assignments 2010, 4, 21–3.
77. Hu KN; Havlin RH; Yau WM; Tycko R, Quantitative Determination of Site-Specific Conformational Distributions in an Unfolded Protein by Solid-State Nuclear Magnetic Resonance. J. Mol. Biol 2009, 392, 1055–1073. [PubMed: 19647001]
78. Siemer AB; Huang KY; McDermott AE, Protein Linewidth and Solvent Dynamics in Frozen Solution NMR. Plos One 2012, 7.
79. Lange S; Linden AH; Akbey Ü; Franks WT; Loening NM; van Rossum BJ; Oschkinat H, The Effect of Biradical Concentration on the Performance of DNP-MAS-NMR. J. Magn. Reson 2012, 216, 209–212. [PubMed: 22285634]
80. Hu KN; Yau WM; Tycko R, Detection of a Transient Intermediate in a Rapid Protein Folding Process by Solid-State Nuclear Magnetic Resonance. J. Am. Chem. Soc 2010, 132, 24–25. [PubMed: 20000466]
81. Linden AH; Lange S; Franks WT; Akbey Ü; Specker E; van Rossum BJ; Oschkinat H, Neurotoxin II Bound to Acetylcholine Receptors in Native Membranes Studied by Dynamic Nuclear Polarization NMR. J. Am. Chem. Soc 2011, 133, 19266–19269. [PubMed: 22039931]

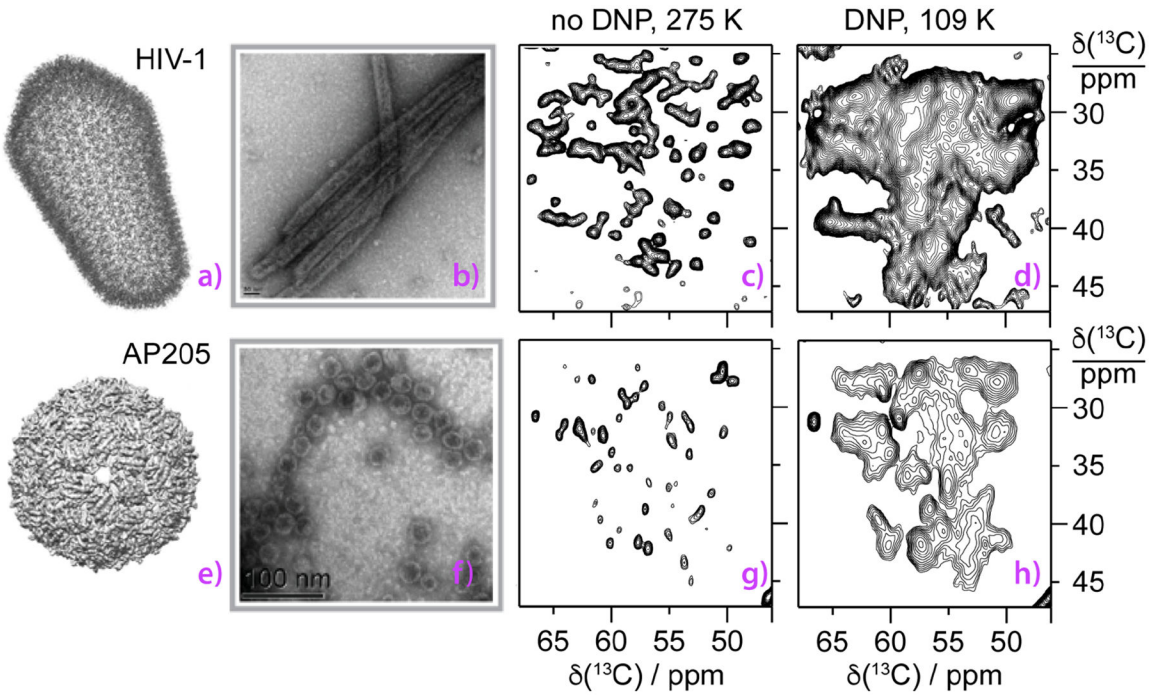

Figure 1.

HIV-1 (top), and bacteriophage AP205 (bottom) viruses investigated by DNP-enhanced MAS NMR spectroscopy. a) an all-atom model of mature HIV-1 capsid (PDB ID: 3J3Y),[65] e) cryo-EM reconstruction of AP205.[58] b,f) transmission electron microscopy (TEM) images. c,d) expansions of ^{13}C-^{13}C correlation spectra of CA tubular assemblies and g,h) AP205 VLPs. Conditions were c) 19.96 T, 277 K; d) 14.1 T, 110 K, DNP-enhanced; g) 23.4 T, 275 k; h) 18.8 T, 109 K, DNP-enhanced. For detailed experimental conditions, see Materials and Methods.

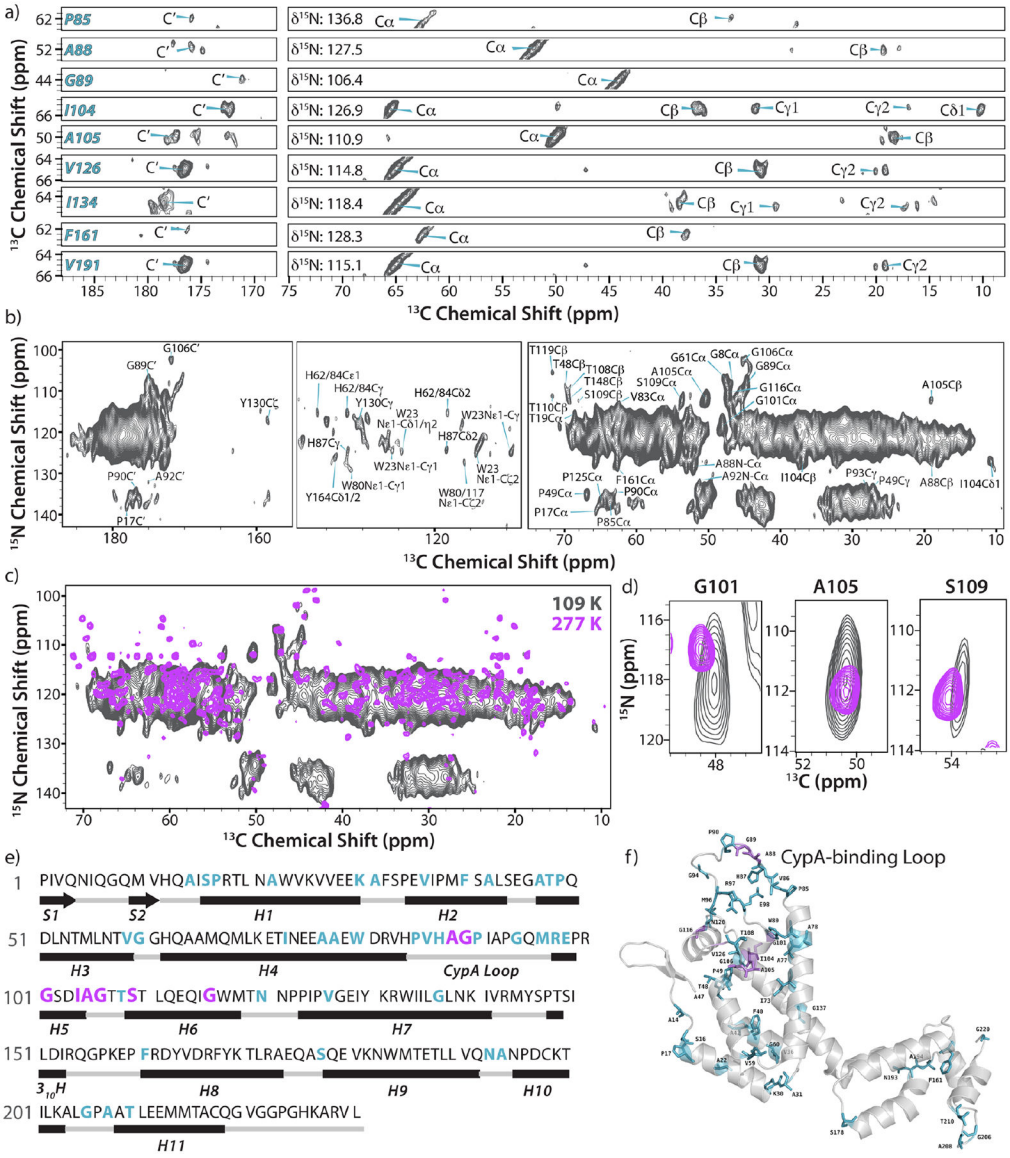

Figure 2.

DNP-enhanced 2D- and 3D NCACX correlation spectra of U-^{13}C, ^{15}N HIV-1 CA tubular assemblies acquired at 14.1 T and 109 K. (a) Selected 2D strips of the 3D NCACX spectrum showing well-resolved resonances and their assignments. (b) 2D NCACX spectrum. The MAS frequency was 12.5 KHz, SPECIFIC-CP time for the NCA transfer was 6.5 ms and the DARR mixing time was 40 ms. (c) Overlay of 2D NCACX spectra acquired under cryogenic temperatures with DNP (14.1 T, gray) and under ambient-temperature conditions without DNP (21.1 T, magenta). (d) An expansion of (c) showing three representative, well-resolved resonances. (e) The primary amino acid sequence of CA with the secondary structure shown. (f) The position of amino acid residues observed and assigned by DNP-enhanced MAS NMR spectroscopy shown in the crystal structure of unassembled full-length CA (PDB: 3NTE). In e)-f), assigned residues are colored cyan and residues for which chemical shift distributions were analyzed are colored magenta.

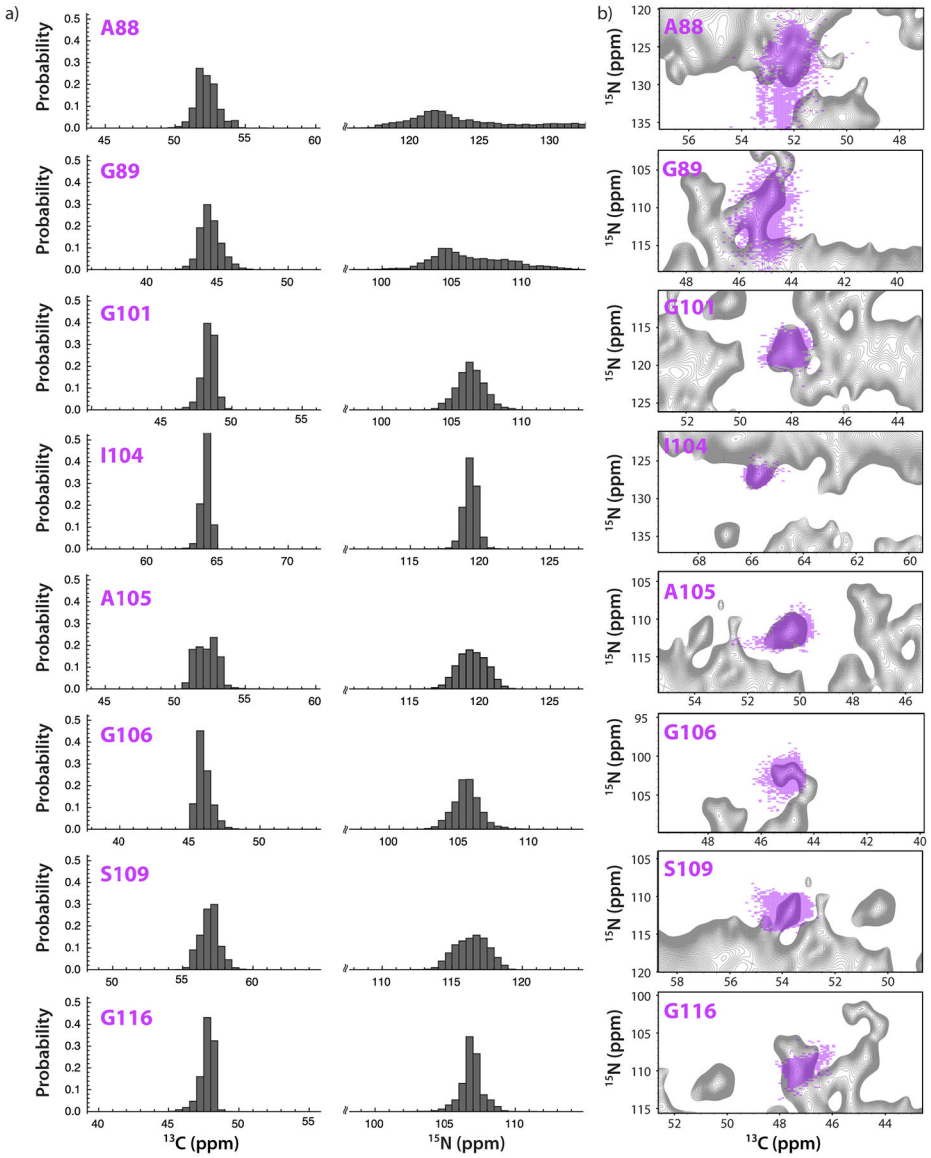

Figure 3.

a) The probability distributions of $^{13}C^{\alpha}$ and $^{15}N^{H}$ chemical shifts, calculated from 5000 substructures of the 100-ns MD trajectory for representative amino acids of HIV-1 CA. The range was set to ±8 ppm of the isotropic chemical shift to demonstrate the relative spread in chemical shift values. The isotropic chemical shifts were calculated using SHIFTX.[61]. b) Overlay of experimental contour plots (light pink) for well-resolved signals in the DNP-enhanced ^{15}N-^{13}C 2D NCACX correlation spectrum and chemical shift distribution maps for the corresponding residues (grey) of of U-^{13}C, ^{15}N HIV-1 CA tubular assembly, calculated from 5000 substructures of 100 ns MD trajectories. Experimental conditions are the same as in Fig. 2.

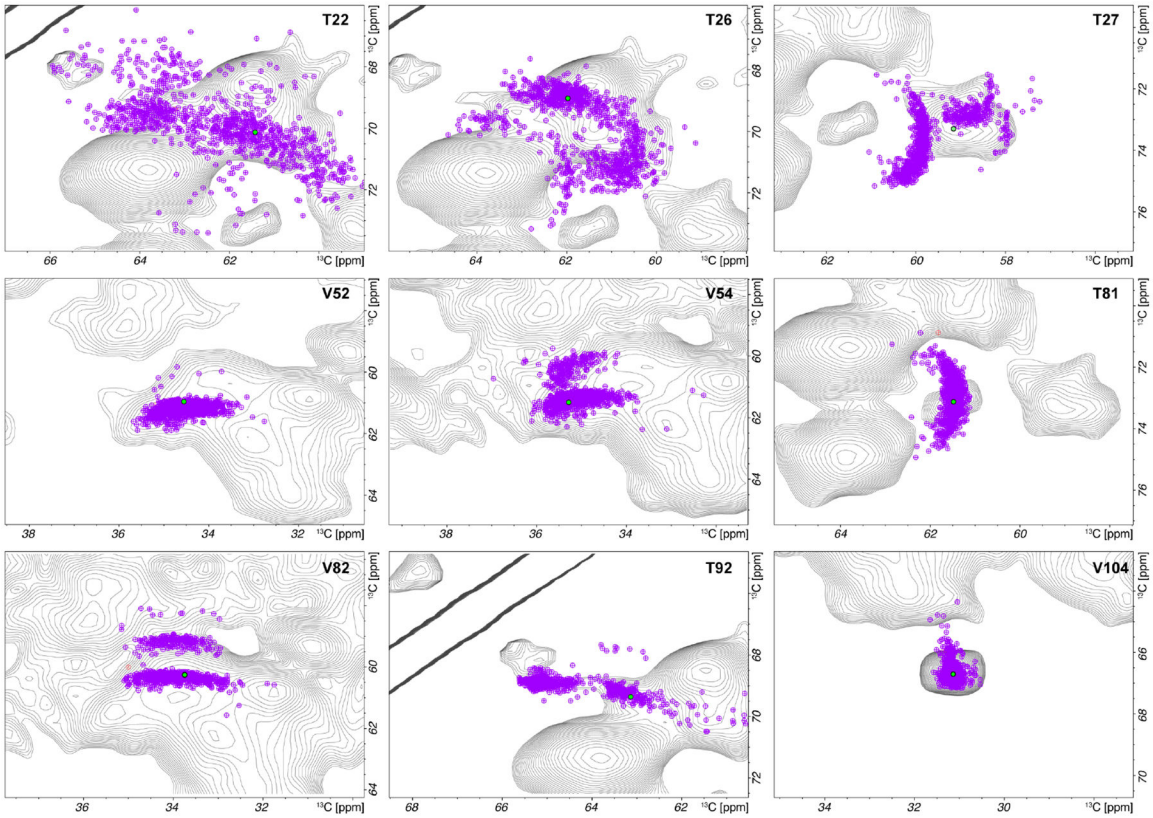

Figure 4.

An overlay of two-dimensional chemical shift maps calculated from MD trajectories and ^{13}C-^{13}C correlations in a DNP-enhanced MAS NMR CORD spectrum of AP205 VLPs.